Biomed Microdevices (2015) 17: 44
DOI 10.1007/s10544-015-9944-y

Drug coated microneedles for minimally-invasive treatment of oral carcinomas: development and *in vitro* evaluation

Yunzhe Ma · Seth E. Boese · Zhen Luo · Nitin Nitin · Harvinder S. Gill

Published online: 20 March 2015

Abstract Treatment of recurring oral cancers is challenging as common surgical approaches are not feasible for these patients. In addition, these patients do not respond well to systemic chemotherapy. Localized intratumoral injection of anti-cancer drugs is considered to be an attractive alternative treatment approach for these patients. However, conventional hypodermic injections result in poor distribution of the drug in the tumor and leakage of the drug from the injection site to systemic circulation, in addition to causing pain to the patient. The objective of this study was to develop coated microneedles as a novel device for direct and minimally invasive intratumoral delivery of anti-cancer drugs. Poly(lactic-co-glycolic) acid (PLGA) nanoparticles encapsulating doxorubicin (DOX) were prepared and coated on inplane (1D) microneedles. Microscopic evaluation of 3D tissue phantoms and porcine cadaver buccal tissues that were treated with 1D microneedle arrays coated with DOX-PLGA nanoparticles demonstrated that DOX could diffuse both laterally and vertically in to the tissues and produced cellular cytotoxicity. Out of plane (2D) microneedle arrays measuring 1 cm x 1 cm with 57 microneedles coated with free DOX could produce uniform distribution of DOX in a porcine cadaver buccal tissue up to a depth greater than 3 mm. Hypodermic injection of different volumes in to a porcine buccal tissue confirmed significant leakage of the injected volume (about 25 % of the injected 80 μl). In summary, this study demonstrates that drug coated microneedles is an attractive microscale device that can uniformly and effectively deliver drugs to localized oral cancers. This microscale device has potential to impact the treatment of oral cancer patients.

Keywords Coated microneedles · Doxorubicin · Intratumoral · Nanoparticles · PLGA

Submitted to *Biomedical Microdevices* for consideration as an Original Research Paper.

Yunzhe Ma and Seth E. Boese contributed equally to this work.

Y. Ma · S. E. Boese · H. S. Gill (✉)
Department of Chemical Engineering, Texas Tech University, 8th Street & Canton Ave, Lubbock, TX 79409-3121, USA
e-mail: harvinder.gill@ttu.edu

Z. Luo · N. Nitin (✉)
Department of Biological and Agricultural Engineering, University of California, Davis, CA 95616, USA
e-mail: nnitin@ucdavis.edu

1 Introduction

Surgical resection combined with radiotherapy and chemotherapy is the frontline treatment for oral cavity tumors (Haddad and Shin 2008; Hancock et al. 2008). Surgical resection can result in significant loss and impairment of function such as difficulty in swallowing and eating, speech, and psychological trauma due to facial cosmetic disfigurement. Even with extensive surgical resection, recurrence rate for oral cancers is high (60–70 %) (Khuri et al. 2000b). Typically, recurring tumors are not amenable to re-surgery or re-radiation; in addition they also fail to respond to systemic chemotherapy. Poor drug delivery to recurring tumors via the systemic route can be due to multiple reasons including a higher pressure inside the tumor, which can range from 5 to 40 mmHg and even as high as 100 mmHg (Curti et al. 1993; Gutmann et al. 1992; Rofstad et al. 2010) compared to -3 to 3 mmHg inside normal tissues (Heldin et al. 2004; Milosevic et al. 2004), abnormalities in tumor vasculature (Raju and Ibrahim 2011), or lack of good vasculature due to a previous resection surgery.

To overcome the inability to treat recurring tumors via systemic chemotherapy, direct administration of anticancer drugs

to tumors has been investigated. Approaches such as intralesional chemotherapy (Goette and Odom 1980) and intratumoral chemotherapy (Smith et al. 1999) have been tested in various cancer models, including squamous cell carcinoma. In an early clinical study, 45 patients who had tumors at different accessible locations such as the tongue, oral pharynx, esophagus and skin, but none of which were eligible for surgery, radiation or systemic chemotherapy, were treated with intratumoral chemotherapy using an injectable gel containing cisplatin, an anti-tumor drug, and epinephrine, a vasoconstrictor to reduce cisplatin's loss into systemic circulation. No cisplatin-related toxicities were observed in the patients, and about 38 % of the patients showed complete response (Burris III et al. 1998). This gel-system was subsequently tested in a phase III study in patients with recurrent or metastatic oral tumors, and the treatment was shown to induce complete or partial response in 34 % of the patients (Castro et al. 2003). In addition to treatment of recurring oral cancers, induction chemotherapy is also considered as one of the options to improve survival in patients with irresectable oral cancers (Hitt 2006; Hitt et al. 2014). Thus, it is envisioned that the localized intratumoral chemotherapy can also aid in surgical planning for tumors which are difficult to resect due to increased risk of loss of vital function.

While these clinical trials and other studies (Clayman et al. 1998; Khuri et al. 2000a; Miyazaki et al. 2011; Nemunaitis et al. 2001) of localized and sustained delivery of anticancer drugs have been shown to be of therapeutic value, significant challenges exist that prohibit its effective use in patients. The most common approach for intratumoral delivery is to use a hypodermic needle to inject the drug, however, multiple limitations exist related to this approach: (i) hypodermic needle injections cause pain (Castro et al. 2003; MacDonald et al. 2009); (ii) drug is irregularly distributed and carefully spaced injections are required to cover the entire tumor volume (French et al. 2010; MacDonald et al. 2008, 2009) making it difficult to implement in a clinical setting; (iii) injection volume and injection pressure must be carefully controlled to prevent leakage from the tumor volume to avoid systemic toxicity, especially when tumors are in close proximity to major blood vessels (MacDonald et al. 2008). Given these current limitations of intratumoral drug delivery, a more versatile and well-engineered modality needs to be developed to further improve intratumoral delivery to help translate it in to clinics.

To address the aforementioned challenges, we hypothesized that microneedles, which are micron-sized structures could be used to deliver anti-cancer drugs to tumors in a minimally invasive and painless fashion (Gill et al. 2008). Microneedles can be used in different configurations for drug delivery; they can be used as hollow microneedles for injection (Norman et al. 2013; van der Maaden et al. 2014; Wang et al. 2013), as solid structures wherein the drug is encapsulated in the microneedle material (Chu et al. 2010; Gittard et al. 2009; Lee et al. 2012; Park et al. 2005; Sullivan et al. 2010), or as coated microneedles (DeMuth et al. 2010; Gill and Prausnitz 2007; Gill et al. 2010; Ma et al. 2014; Widera et al. 2006). We decided to use the coated microneedle approach for intratumoral delivery because this method does not involve fluid injection, and can thus minimize convection-based drug loss from the tumor in to systemic circulation. In the coated microneedle approach, a water soluble polymer containing the drug is coated on to microneedles whose subsequent insertion into tissues results in dissolution of the film in the interstitial fluid leading to deposition of the drug at points of microneedle insertions. A microneedle patch measuring a centimeter long and a centimeter wide can accommodate tens of closely spaced microneedles, typically 0.5 to 2 mm apart. Over time, diffusion of drug from these closely spaced drug depots could create uniform drug distribution within the tumor. Previous research has demonstrated that polymeric particles can be engineered to achieve high encapsulation efficiency and the desired release rate of anti-tumor drugs (Shahani et al. 2010). Previously it has also been shown that microparticles can be coated on microneedles and can be successfully delivered in to tissues (Gill and Prausnitz 2007). Thus, to enable long term local treatment of tumors we also sought to include nanoparticles in the microneedle coatings that can provide sustained drug release. Accordingly, this study establishes the proof-of-principle to use coated microneedles for intratumoral drug delivery by developing microneedles coated with doxorubicin (DOX)-encapsulating PLGA (DOX-PLGA) nanoparticles and characterizing them *in vitro* in a 3D tissue phantom model and porcine buccal tissue.

2 Materials and methods

2.1 Materials

Doxorubicin hydrochloride salt (MW: 579) was purchased from Biotang (MA, USA). Poly (D, L-lactide/glycolide copolymer), having a lactide/glycolide molar ratio of 50/50 and an average molecular weight of 40–75 kDa, was a kind donation from Purasorb (Gorinchem, Netherlands). Poly(vinyl alcohol) (MW 13–26 kDa) was purchased from Sigma-Aldrich (USA). Other chemicals involved in nanoparticle synthesis were of reagent grade and obtained from Thermo Fisher Scientific (USA), MP Biomedicals (Aurora, OH, USA), and Sigma Chemicals (USA). Solutions were prepared in Milli-Q water. Microneedles were etched from stainless steel sheets. Porcine cadaver buccal tissue was purchased from Innovative Research (MI, USA).

2.2 Synthesis of DOX-encapsulating PLGA nanoparticles

DOX-loaded PLGA nanoparticles were prepared using a double emulsion w/o/w technique, as previously described (Tewes et al. 2007). Briefly, aqueous DOX (25 mg of DOX HCl dissolved in 500 μl of deionized water) was emulsified with the organic phase (100 mg of PLGA dissolved in 2 ml of dichloromethane) by probe sonication for 30 s at 38 % amplitude at 500 W in an ice bath using a half-inch ultrasound probe from Fisher Scientific (PA, USA) to form the w/o phase. The primary emulsion was then added drop-wise to 4 ml of 1 % (*w*/*v*) poly(vinyl alcohol) (PVA) aqueous solution at room temp under magnetic stirring at 500 rpm and sonicated using the same conditions as used for w/o phase, to form the w/o/w emulsion. The double emulsion was next diluted into 20 ml of 0.1 % (*w*/*v*) aqueous PVA and magnetically stirred at 350 rpm overnight to remove dichloromethane. The nanoparticles were washed and centrifuged for 10 minutes at 18,000 rpm three times for the removal of free DOX and residual PVA. The drug-loaded nanoparticles were then freeze-dried (Virtis Benchtop Freeze-Dryer, SP Scientific, Warminster, PA, USA).

2.3 Microscopic examination, encapsulation efficiency, and release kinetics of nanoparticles

Morphology of nanoparticles was characterized by scanning electron microscopy (SEM) using Hitachi S-3400 (Hitachi, Tokyo, Japan). Size of DOX-PLGA nanoparticles was assessed using SEM and dynamic light scattering (DLS) using the Zetatrac (Microtrac Inc., PA, USA).

Drug encapsulation efficiency (EE) defined as the ratio between encapsulated drug and initial drug mass used, and drug loading efficiency (LE) defined as mass of encapsulated drug per unit mass of nanoparticles was determined by taking a known amount of freeze-dried DOX-PLGA nanoparticles and completely dissolving them in DMSO with 2 μl of acetic acid to compensate for basicity. Concentration of the drug was measured using a fluorescence spectrophotometer (Cary Eclipse, Agilent Technologies, Santa Clara, CA, USA) with excitation and emission wavelengths of 480 and 550 nm respectively. The drug concentration of the solution was calculated using a standard calibration curve prepared from solutions with known concentrations of DOX in DMSO.

Release kinetics of DOX from DOX-PLGA nanoparticles was analyzed using the dialysis technique. A known mass of DOX-PLGA nanoparticles was added to a cellulose membrane dialysis tubing, which was then placed in 20 ml phosphate buffered saline (PBS). The volume was stirred at 37 °C, and at different time intervals, 1 ml solution was collected and replaced with 1 ml fresh PBS. Fluorescence spectrophotometry was used to determine mass of released DOX in the collected samples to calculate cumulative release. Although the *in vitro*, *ex vivo*, and *in vivo* release kinetics may differ, the *in vitro* release profile is still widely used as a basis to evaluate nanoparticle formulations (Jain 2000).

2.4 Microneedle fabrication and dip-coating with DOX-PLGA nanoparticles

Planar 1-dimensional (1D) arrays containing five microneedles in a row were fabricated from 50 μm-thick stainless steel (SS316) sheets using a wet etching process. Each microneedle measured 700 μm in length and 200 μm in width. Similarly, 2D microneedle patches measuring 1 cm x 1 cm with 57 microneedles of the same dimension as the 1D array were also fabricated. Microneedles were coated with DOX-PLGA nanoparticles as described before using a computer-controlled micro-precision coating device (Gill and Prausnitz 2007; Ma et al. 2014). Coating solution included 1 % (*w*/*v*) carboxymethylcellulose sodium salt (low viscosity, USP grade, CarboMer, San Diego, CA, USA), 0.5 % (*w*/*v*) Lutrol F-68 NF (BASF, Mt. Olive, NJ, USA), and 10 % (*w*/*v*) DOX-PLGA nanoparticles.

2.5 Amount of DOX as DOX-PLGA nanoparticles coated on microneedles and its delivery efficiency into buccal tissue *in vitro*

To determine the amount of DOX coated on microneedles, three 1D microneedle arrays coated with DOX-PLGA nanoparticles were placed in 200 μl of 0.1 M NaOH aqueous solution and agitated with a vortex device to dissolve the nanoparticles. This procedure was repeated two more times to obtain triplicate samples. DOX concentration (C_1 as μg/ml) in 200 μl volume was determined using fluorescence spectroscopy and a standard curve, which was prepared using known concentrations of DOX in 0.1 M NaOH. C_1 was then converted in to mass of DOX coated per 1D array (M_1 as μg) using the formula (C_1*0.2 ml)/3.

To determine delivery efficiency, that is, the fraction of microneedle-coated DOX-PLGA nanoparticles delivered into tissue, six nanoparticle-coated 1D microneedle arrays were each inserted into porcine cadaver buccal tissue. After 5-min of insertion the arrays were removed and placed into 200 μl of 0.1 M NaOH solution and agitated with a vortex device to dissolve the DOX-PLGA nanoparticles still attached to microneedles to create a DOX solution with concentration C_2. The particles that were detached from the microneedle surface were assumed to be either delivered in to the tissue or deposited on the tissue surface (Gill and Prausnitz 2007). A cotton-tipped applicator, moistened with 0.1 M NaOH was used to collect any residual DOX-PLGA nanoparticles from the tissue surface and placed in a microcentrifuge tube containing 200 μl of 0.1 M NaOH to dissolve the nanoparticles collected from the tissue surface to create a DOX solution with concentration C_3. After a brief period the applicator was

removed by first firmly pressing the tip against the sides of the microcentrifuge tube to ensure removal of entrained liquid. This process was repeated a total of three times to obtain samples in triplicate. Calibrated fluorescence spectroscopy as described above was used to determine concentrations C_2 and C_3 in μg/ml, which were then used to calculate mass of DOX left on microneedles (M_2) and on tissue surface (M_3) normalized to one 1D array using the formulas (C_2*0.2 ml)/6 and (C_3*0.2 ml)/6, respectively. Delivery efficiency was then calculated as (M_1-M_2-M_3)/M_1*100.

2.6 Design of 3D tissue phantom model

3D tissue models were prepared using cancer cells (HeLa cancer cell line) embedded in a collagen matrix. Type I collagen (Roche USA) was dissolved in 0.2 % acetic acid to 3 mg/mL. To prepare a 3D tissue model with high cell density, a suspension of cancer cells was spun down and resuspended in a small volume of Dulbecco's modified Eagle's medium (DMEM) media (Invitrogen, Carlsbad, CA) containing 5 % fetal bovine serum (FBS) to reach a cell density of 1×10^8 cells/mL. The collagen solution and cell suspensions were then mixed in a 2 to 1 ratio (by volume) to obtain a final collagen concentration of 2 mg/mL. 1 M NaOH was gradually added into the mixture to achieve a final pH of 7.4. Then the suspension was transferred into a 24 mm transwell with a 3.0 μm pore polycarbonate membrane at the bottom (Corning Incorporated, Corning, NY). These transwells were then placed in a 24-well plate with 500 μl of DMEM containing 5 % FBS. The collagen-cell matrix was allowed to gel at 37 °C for 30 minutes. After forming the tissue model, 40 μl of cell culture media was added to the top of the model. Tissue models were incubated at 37 °C for approximately 48 hours. This incubation promotes the formation of a highly dense 3D tissue model (total volume of approximately 140 μl). The tissue phantoms measure approximately 6.5 mm in diameter and 3–4 mm in height.

2.7 Measurement of DOX diffusion and cytotoxicity in 3D tissue phantoms after delivering DOX-PLGA nanoparticles using coated microneedles

Microneedles coated with DOX-PLGA nanoparticles were inserted into 3D tissue phantoms for 5 min and removed. Post insertion, the tissue phantoms were incubated for 4 h at 37 °C. After incubation, the tissue phantoms were imaged using two complementary approaches to map the distribution of DOX in the model tissue. In the first approach, the intact tissue phantom was imaged using confocal microcopy (Zeiss Upright Confocal Microscope) to map the radial distribution of DOX with respect to the insertion point. In the second approach, the tissue phantom was transversely sectioned and the individual sections were imaged using confocal microscopy to map distribution of DOX along the depth of the tissue phantom. Transverse sections were prepared by embedding tissue models in 5 % agar gel (*w*/*w*%) and transversely sectioning the gels using an oscillating tissue slicer (EMS 5000, Electron Microscopy Sciences Inc., Hatfield, PA). For both these imaging measurements, the tissue phantoms were imaged using a 488 nm laser excitation and the emission signal was collected using a band pass emission filter (550–620 nm). NIH Image J software was used for the quantitative analysis of the imaging data. To quantify the mean fluorescence intensity, the RGB images were converted to the grey scale images and the mean fluorescence intensity over a selected region of interest was quantified.

Functional efficacy of DOX-PLGA delivered into 3D tissues was assessed by evaluating its cytotoxic effect. A set of tissue phantoms treated with microneedles coated with DOX-PLGA nanoparticles were incubated for 48 h post microneedle insertion and then topically labeled with propidium iodide (a cell viability stain, which fluoresces in dead cells) at a concentration of 1 μg/ml, and Annexin-FITC (an apoptosis stain, which fluoresces in apoptotic cells) for 30 minutes to assess cellular cytotoxicity. Following topical labeling the phantoms were washed using PBS. The washed phantoms were imaged using a confocal unit with an excitation/emission of 543/580 nm and 488/520 nm for propidium iodide and Annexin-FITC, respectively. Tissue phantoms treated identically but with uncoated microneedles were used as a negative control.

2.8 Diffusion of DOX in porcine oral mucosal tissue using 1D and 2D microneedle arrays

Underlying fat and connective tissue of porcine cadaver buccal tissues was partially removed to obtain 3.5 to 4.3 mm thick samples. Tissue thickness was confirmed using a digital caliper. A 1D array coated with DOX-PLGA nanoparticles was inserted in porcine buccal tissue and held for 5 minutes. The post-insertion buccal tissues were stored at 37 °C for 4 h to allow DOX to release and diffuse in the tissue over time. The 4 h incubation time for oral tissues was selected to be consistent with the incubation time for tissue phantoms, however, we acknowledge that the nanoparticle drug release kinetics between the two could be different. Subsequently the tissue was transversely sectioned and imaged using the same procedure as used for the tissue phantoms. To characterize penetration depth of the DOX in the tissues, an image mosaic was constructed by combining the individual image frames of the transverse tissues. To characterize the variation in fluorescence intensity corresponding to distribution of DOX in the tissue, the image mosaic was divided into sections of 100 micron width and the mean fluorescence intensity at each 100 μm depth was obtained using Image J.

In another experiment a 2D microneedle array coated with free DOX (not encapsulated in PLGA nanoparticles) was inserted into porcine buccal tissue for 5 min and removed. The tissue was incubated in a moist petridish with the bottom side of the tissue (side opposite to epithelial surface) placed in direct contact with a moist tissue paper at 37 °C for 24 h. Brightfield and fluorescent images of the top (epithelium) and back side of the tissue were collected just before insertion, just after insertion and after incubation for 24 h, using a fluorescent stereomicroscope (SZX16, Olympus America Inc., Center Valley, PA, USA). All images were collected using the identical settings.

2.9 Measurement of leakage from porcine buccal tissue after hypodermic injection

Porcine cadaver buccal tissues 3.5 to 4.3 mm thick were obtained as described above. Tissues measuring slightly larger than the diameter of a 15 ml conical tube cap were cut. An outline of the 2D microneedle array was marked on the epithelial surface of these tissues and placed over and across a conical tube cap containing 2.1 ml Milli-Q water. Volumes of 20, 40, 60, or 80 μl containing 4.2 mg/ml of DOX dissolved in Milli-Q water were injected within the outlined area at the approximate mid-point depth using a 30 gauge insulin-syringe inserted at an angle. Each injection was conducted at a slow and consistent rate and performed in triplicate for the respective injection volumes. Care was taken during insertion so that the needle did not fully pierce the tissue. Using fluorescence spectroscopy and a standard curve, amount of DOX that leaked into the water in the cap was measured and reported as a percentage of injection volume.

3 Result and discussion

3.1 Design of coated microneedles to achieve widespread distribution of drugs in tumors

We hypothesized that by depositing anti-tumor drugs in tumor tissues at densely-packed locations using coated microneedles, a uniform distribution of the drug inside the tumor could be achieved due to overlapping diffusion fronts developing from the individual drug depots (Fig. 1a). Guided by our previous study (Luo et al. 2013) where we had demonstrated that 1D microneedle arrays with an inter-microneedle spacing of 1.5 mm led to widespread distribution of oligonucleotides in tissues, we decided to test similar microneedle spacings in this study. We used a 1D microneedle array with a microneedle spacing of 1.5 mm and a span of 6 mm (Fig. 1b), which was adequate for insertion into tissue phantoms measuring 6.5 mm in diameter for *in vitro* assays. We also designed 2D arrays with 57 microneedles (Fig. 1c and d) arranged in a rhombus-pitch with equilateral sides of 1.3 mm and two diagonals measuring 1.83 mm (within row spacing) and 0.92 mm (1.83/2 = 0.92; inter row spacing) to enable characterization in larger porcine cadaver buccal tissues.

3.2 DOX-PLGA nanoparticles

3.2.1 Size

PLGA is an FDA approved biodegradable polymer with sustained release qualities (Jain 2000), and was thus used to prepare DOX-encapsulating nanoparticles. As revealed by SEM (Fig. 2a), the double emulsion synthesis provided smooth, spherical particles with a uniform size. Despite use of accelerating voltages as low as 2.0 kV, beam damage on the particles was still observed (Fig. 2a). Particle size was further confirmed through DLS analysis. From Fig. 2b it can be seen that particles have a monomodal size distribution ranging from 102 to 243 nm. Although a population of less than 1 % of the particles had a diameter greater than 243 nm, majority of the particles synthesized ranged in diameter from 122 to 172 nm with an average of 137 nm.

3.2.2 Encapsulation efficiency, loading efficiency and release kinetics

We selected DOX as the anti-tumor drug because it is fluorescent and offers ease of imaging and detection. However, due to its hydrophilic nature, DOX.HCl is a difficult molecule to encapsulate into PLGA particles (Tewes et al. 2007). An EE and LE of 4.41 and 1.8 %, respectively was observed for the DOX-PLGA nanoparticles. To evaluate sustained release, the release kinetics of DOX from DOX-PLGA nanoparticles was assessed over a 24 h period (Fig. 2c). From Fig. 2c it is seen that the nanoparticles rapidly release about 30 % of the encapsulated DOX within the first 3 h, and then slowly releases 34 % over the 24 h period. This sustained release of DOX, especially the release of the remaining 66 % of the drug still contained within the nanoparticles is a beneficial trait for chemotherapy because constant exposure of tumor cells to DOX is expected to result in high cytotoxicity.

3.3 Amount of DOX in the form of DOX-PLGA nanoparticles coated on microneedles and its delivery efficiency into porcine buccal tissue *in vitro*

To achieve cytotoxic effects in tumors, it is critical to coat microneedles with sufficient DOX-PLGA nanoparticles such that the DOX concentration in tumors can be above the toxic limit. Figure 3a and b show SEM images of the naked and coated microneedles. Exploiting fluorescence of DOX, DOX-PLGA nanoparticles were also imaged using fluorescence microscopy as shown in Fig. 3c. Both SEM and fluorescence

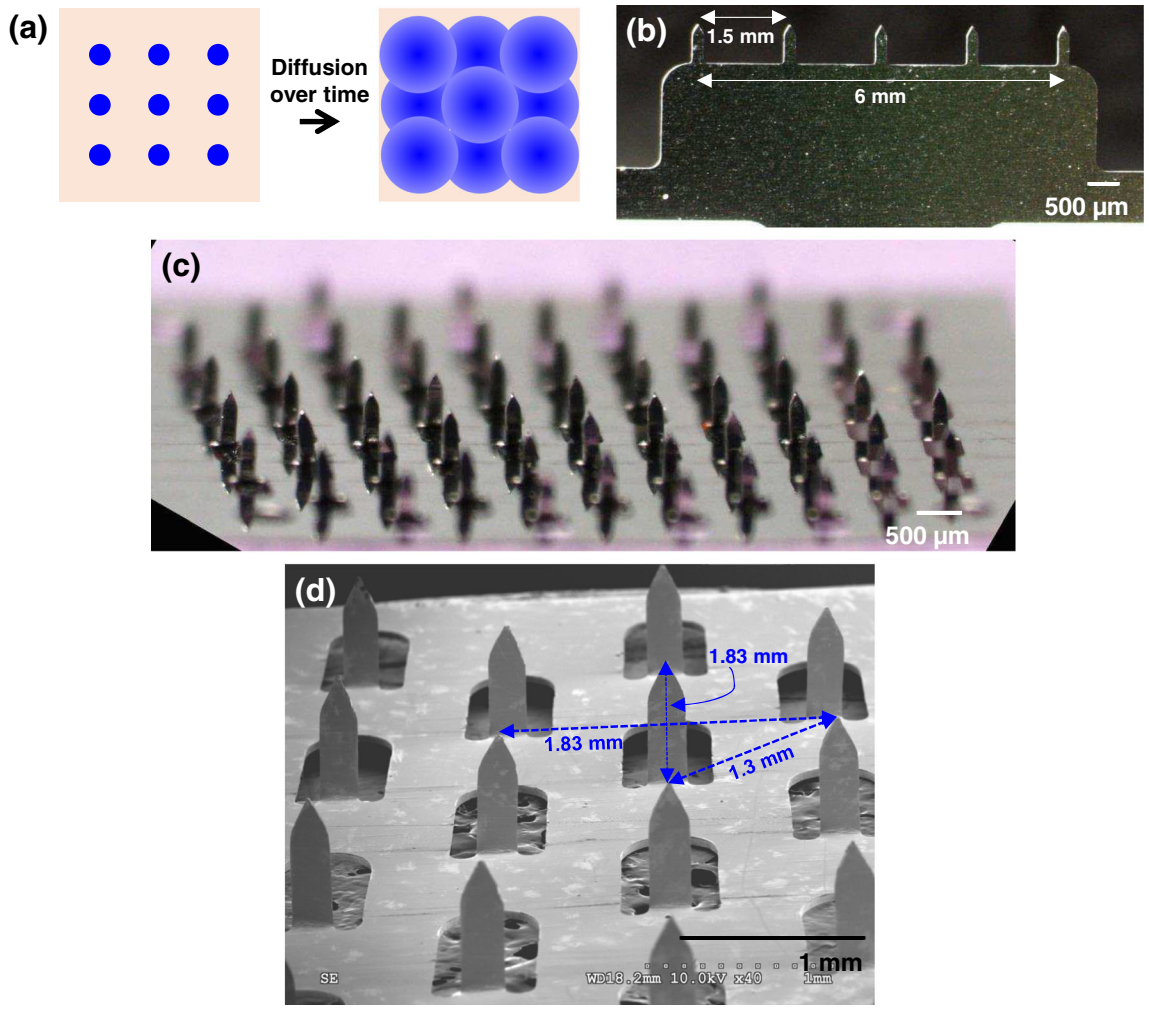

Fig. 1 Microneedles for intratumoral drug delivery. (**a**) Schematic describing the concept of diffusion-based distribution of anti-cancer drug in a tissue. Deposition of drug at controlled geometric locations in tissue will facilitate diffusion of drug molecules from the deposited drug sources. At appropriate spacing between the drug deposition points, overlap between diffusion fronts can occur resulting in a relatively uniform drug distribution in tissue over large surface areas. (**b**) Brightfield micrograph of a 1D microneedle array. (**c**) Brightfield micrograph of a 2D microneedle array. (**d**) Scanning electron micrograph of a section of a 2D microneedle array showing microneedle spacing

imaging indicate a relatively uniform coating of the microneedle with PLGA-DOX nanoparticles. The amount of DOX loaded per 1D microneedle array in the form of DOX-PLGA nanoparticles was quantified as described in the materials and methods section. It was found that 0.6±0.18 μg DOX could be coated onto a single 1D microneedle array. The toxicity for DOX in human solid prostate tumors *in vivo* is 1 μM, that is, 0.58 μg/cm^3 (Chen et al. 1998). Assuming similar toxicity for oral tumors and a tumor volume of 1 cm^3, a total of 0.58 μg DOX will be required to attain toxic level of DOX. This amount can be delivered using a single 1D array, which on average is coated with 0.6 μg DOX. However, practically, to treat a large tumor surface measuring 1 cm x 1 cm in size, a 2D microneedle array would be utilized, which contains almost 10-fold more microneedles than a 1D array, and would thus help to deliver a significantly higher dose of DOX. This data demonstrates that a clinically-relevant dose of DOX as DOX-PLGA nanoparticles can be coated on to microneedles. It is also possible to suspend DOX-PLGA nanoparticles in a coating solution that further contains free DOX. The resulting microneedle coating would then be able to deliver a burst of DOX at high concentration as free drug, supplemented with sustained release of DOX from PLGA nanoparticles.

We next evaluated the percentage of DOX (in the form of DOX-PLGA nanoparticles) coated on microneedles, that gets delivered into tissues. As observed from the fluorescent image of the microneedle post-insertion (Fig. 3d), most of the DOX-encapsulated nanoparticles are removed from the microneedle surface. Quantification indicates 85.6 % of the DOX as DOX-PLGA nanoparticles was delivered into the tissue, while 6.07 and 8.3 % remained on the tissue and microneedle surfaces, respectively (Fig. 3e). This delivery efficiency is consistent with other studies using microneedles (Gill and Prausnitz 2007; Kim et al. 2010).

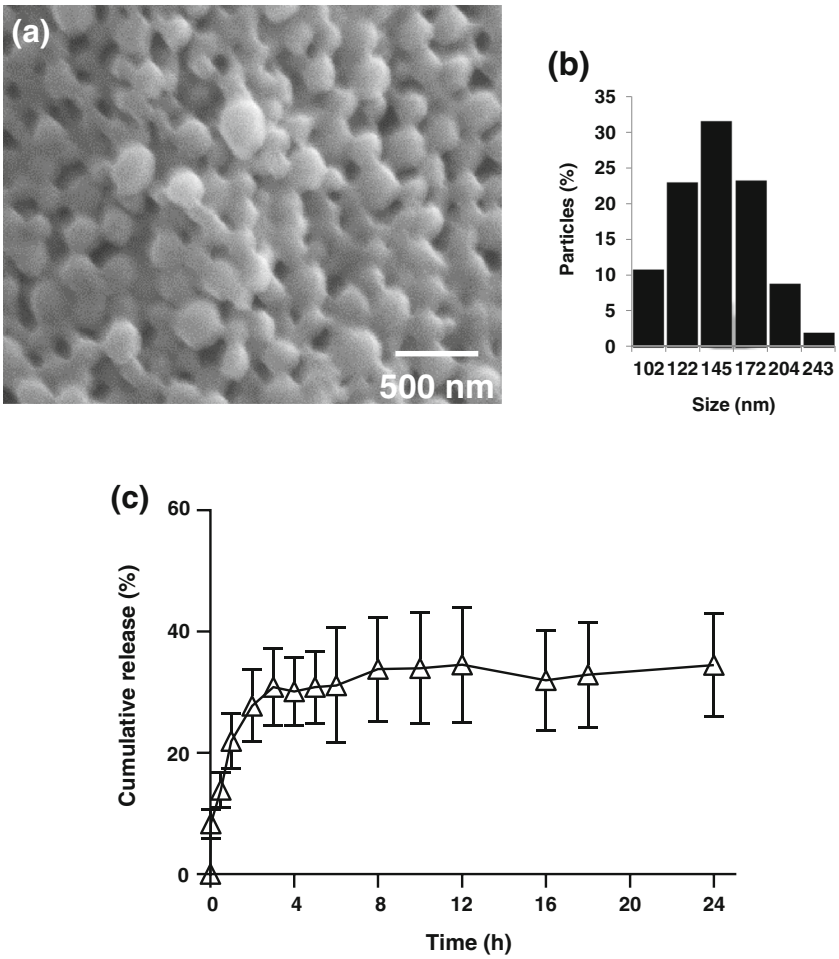

Fig. 2 Characterization of DOX-PLGA nanoparticles. (**a**) Scanning electron micrograph of DOX-PLGA nanoparticles. (**b**) Size distribution of DOX-PLGA nanoparticles measured using dynamic light scattering. (**c**) Cumulative release profile of DOX-PLGA nanoparticles

3.4 Widespread distribution of DOX in 3D tissue phantoms upon delivery of DOX-PLGA nanoparticles using coated microneedles

Microneedle arrays have the ability to deposit DOX-PLGA nanoparticles within close proximity (~1-2 mm apart) of each other. An overlap of diffusion fronts from such closely-spaced drug depots could facilitate rapid distribution of DOX in tissues. Microneedles (1D array) coated with DOX-PLGA nanoparticles were inserted into 3D tissue phantoms. Using confocal microscopy, intra-tissue distribution of DOX was measured along the radius and depth of tissues. The radial distribution of DOX was measured using intact 3D tissue models, while the intra-tissue distribution of DOX along the depth was measured using a transverse section of a tissue model as described in the materials and methods section. Tissue phantoms are a good model for 3D tumor tissues. Previous studies have shown that structural and optical properties (Chauhan et al. 2009; Ramanujan et al. 2002; Sokolov et al. 2002), and diffusion properties of macromolecules in this 3D tissue model are in agreement with measurements in tumor tissues (Brown et al. 2004; Leddy et al. 2006).

Figure 4a is a representative radial confocal scan of the model tissue at a depth of around 30 μm. It can be seen that DOX-PLGA nanoparticles are deposited in the tissue at the site of microneedle insertion. Within a short incubation time of just 4 h, DOX diffused to at least 2 mm from the insertion site. However, as observed from Fig. 4b the mean fluorescence intensity decreased after 1 mm from the point of insertion. It is important to note that the radial direction selected for evaluation of DOX diffusion was perpendicular to the plane of microneedle insertion. Consequently, the measured distance up to which DOX can readily diffuse in a short time (4 h) is largely a result of diffusion from deposit made by a single microneedle of the 1D array. Since the mean fluorescence intensity in this diffusion front suddenly dropped after 1 mm, it can be inferred that if two microneedles are spaced a little less than twice this distance, that is less than 2 mm, their diffusion fronts will each extend 1 mm outward and overlap, allowing DOX to uniformly distribute in the tissue. Thus, the microneedle spacing of 1.5 mm in the 1D array is suitable to achieve uniform distribution of DOX. In comparison to DOX, we have shown in our previous study (Luo et al. 2013) that oligonucleotides delivered into tissue phantoms could diffuse to only 300–500 μm from the insertion site. This difference in diffusional mobility between DOX and oligonucleotides is expected because the oligonucleotides are negatively charged and had a higher molecular weight (6000–7000 Da) than DOX (580 Da).

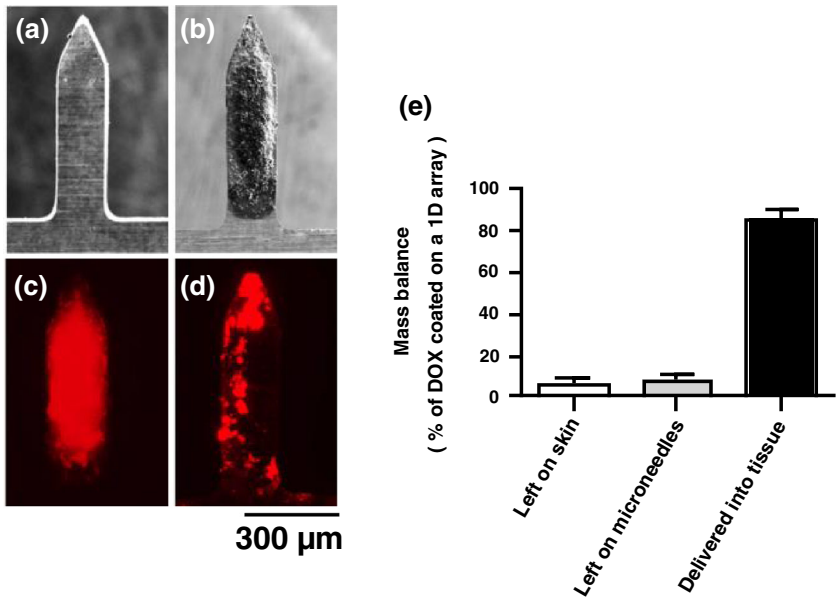

Fig. 3 Characterization of DOX-PLGA nanoparticle coated 1D microneedle array. Scanning electron micrograph of a representative 1D microneedle array (**a**) before and (**b**) after coating with DOX-PLGA nanoparticles. Fluorescence micrograph of a representative 1D microneedle array coated with DOX-PLGA nanoparticles (**c**) before and (**d**) after insertion into porcine cadaver buccal tissue. (**e**) Percent of DOX delivered into tissue, and left on tissue and microneedle surfaces after insertion of DOX-PLGA coated 1D microneedle array into porcine cadaver buccal tissue

Next, the depth to which DOX can diffuse into a 3D phantom was evaluated. Three vertical representative sections of the tissue, one obtained from approximately the middle of the tissue and the other two approximately 2–3 mm away from the middle were visualized. All three sections had similar intensities along their depth. Figure 4c shows representative images for each section, and Fig. 4d shows the mean fluorescence intensities. It can be inferred that, DOX released from the nanoparticles was able to diffuse along the entire depth of the tissue phantom. This result indicates that DOX is rapidly released from DOX-PLGA nanoparticles and dispersed upon insertion of the microneedles in tissue models. The control tissue phantom showed no significant autofluorescence signal using the same imaging settings (data not shown).

3.5 Cytotoxic effect of DOX-PLGA nanoparticles in 3D tissue phantoms

We next investigated whether DOX-PLGA nanoparticles delivered in to 3D tissue phantoms can result in cell death. DOX-

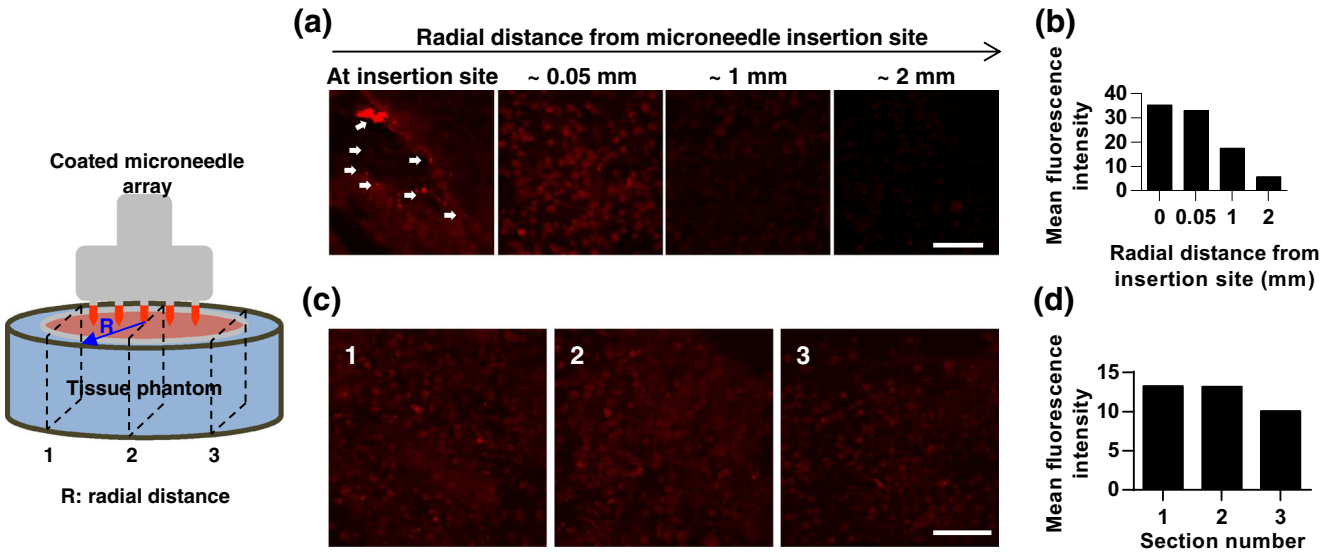

Fig. 4 Delivery of DOX in 3D tissue phantom models after insertion of 1D microneedle arrays coated with DOX-PLGA nanoparticles. (**a**) Confocal fluorescent micrographs characterizing the radial distribution of DOX in an intact 3D tissue model as a function of distance from the microneedle insertion point (*white arrows*). Distances are calculated from the microneedle insertion point in a tissue phantom to the center of the adjacent regions. (**b**) Variation in the mean fluorescence intensity as a function of radial distance from the insertion site. (**c**) Confocal fluorescent micrographs characterizing the distribution of DOX in a transverse cross-section of a tissue. (**d**) Variation in the mean fluorescence intensity averaged across each section demonstrating uniformity of DOX distribution. *Scale bars* in (**a**) and (**c**) represent: 100 μm, and apply to all figures in (**a**) and (**c**), respectively

PLGA nanoparticles coated on 1D microneedle arrays were delivered into 3D tissue phantoms. After 48 h the tissues were stained with two cell viability dyes, propidium iodide and Annexin-FITC. The pseudo green colored image of the tissue phantom upon propidium iodide staining (Fig. 5) shows that there is consistent loss in cell viability indicated by permeation of propidium iodide dye in to individual cells within the phantom tissue. Mechanistically, DOX suppresses tumor cell proliferation by entering the cell nucleus and then inducing single-strand breaks in DNA, thus inhibiting RNA synthesis and causing apoptosis of the cell (Fornari et al. 1994; Mizutani et al. 2005; Müller et al. 1997). Thus, to further verify cell death caused by DOX, we confirmed that apoptosis occurred in cells of the tissue phantom as indicated by positive staining of DOX-PLGA treated tissue phantoms with Annexin-FITC dye, which is a fluorescent molecular indicator of cell apoptosis. Negative control samples of tissue phantoms that were treated with uncoated microneedles did not show positive staining with propidium iodide or Annexin-FITC, demonstrating that the cell death is caused by DOX-PLGA nanoparticles and not by microneedles.

3.6 Depth of DOX diffusion in porcine cadaver buccal tissue

Having demonstrated effective diffusion and cytotoxic effect in 3D tissue phantoms, we next sought to assess the extent of DOX diffusion in porcine buccal tissues whose structure and permeability properties resemble that of humans (Devries et al. 1991; Wertz and Squier 1991), and is widely used as a model for *in vitro* oral drug delivery studies (Kulkarni et al. 2010).

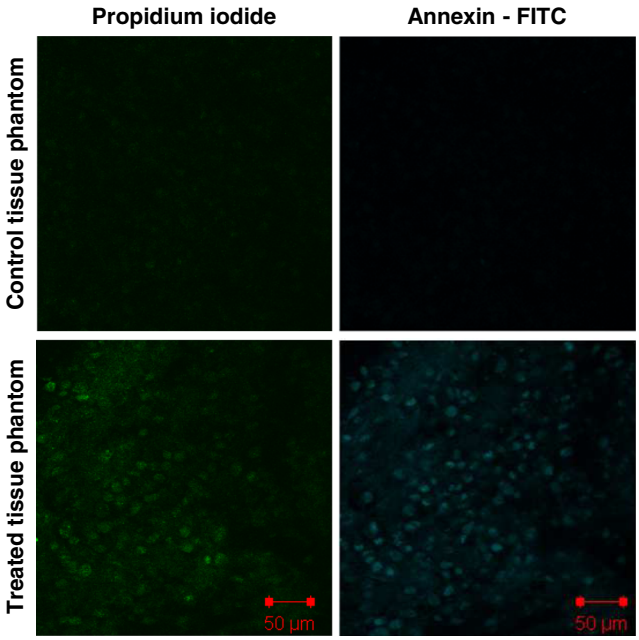

Fig. 5 Cytotoxic response in 3D tissue phantom models after insertion of 1D microneedle arrays coated with DOX-PLGA nanoparticles. Confocal fluorescent micrographs characterizing cell death in an intact 3D tissue model. The propidium iodide staining indicates increased permeability of cell membrane and the Annexin-FITC staining is an indicator of apoptosis

First we evaluated diffusion depth of DOX from DOX-PLGA nanoparticles over a short time frame. A 1D microneedle array coated with DOX-PLGA nanoparticles was inserted into a porcine buccal tissue for 5 min, and the tissue was incubated at 37 °C for 4 h and sectioned. The image mosaic of Fig. 6 shows the depth profile, and it is seen that DOX from DOX-PLGA nanoparticles could diffuse as deep as 1.3 mm. As was seen in 3D tissue phantoms, DOX primarily stained the cells. This is because once DOX enters the cells it binds tightly to the DNA causing DOX to preferentially concentrate in the cells. Because there is reduction in cell density from the epithelium layer to the submucosa, the latter chiefly comprising of connective tissue, the number of stained cells are also seen to reduce in number, deeper into the tissue.

Next, we sought to investigate if longer diffusion times and drug loaded 2D microneedle arrays could lead to uniform distribution of DOX both laterally and deeper in to a tissue measuring 1 cm x 1 cm and about 4 mm thick. We used whole tissue fluorescence imaging using a stereomicroscope for this experiment to map the intra-tissue distribution of the drug. Due to enhanced background from the tissue, stereomicroscopy set-up was not able to distinctly detect fluorescence signal from DOX encapsulated in PLGA nanoparticles. Accordingly, we coated 2D microneedles with free DOX instead of DOX-PLGA nanoparticles with the aim of providing a large bolus dose of DOX, which would permit direct tissue visualization using a stereomicroscope within 24 h of tissue incubation. We note that diffusion of free DOX would be more rapid compared to DOX released from nanoparticles, which can take days to weeks. Since *ex-vivo* tissues cannot be maintained for an extended duration, free DOX thus provides a good model to study diffusion in tissues as compared to DOX encapsulated in PLGA nanoparticles. A 2D microneedle array was uniformly coated with free DOX (Fig. 7a). A representative zoomed section of one of the individual microneedle coated with free DOX is shown in Fig. 7b. Using calibrated florescence spectroscopy it was found that 1.38±0.59 mg of free DOX was coated on a 2D microneedle array with 57 microneedles. The delivery efficiency of free DOX-coated microneedles into porcine cadaver tissue was determined using the same approach as for DOX-PLGA nanoparticle coated microneedles, and was found to be 67 %.

As observed from Fig. 7c, before microneedle insertion, the brightfield and fluorescent images show a clean and DOX-free piece of tissue on both the front and bottom surfaces. Immediately after insertion of a 2D microneedle array coated with free DOX, the insertion points were clearly visible on the top surface of the same tissue under both brightfield and fluorescent imaging, demonstrating delivery of DOX into the tissue. The bottom surface of the tissue did not exhibit any

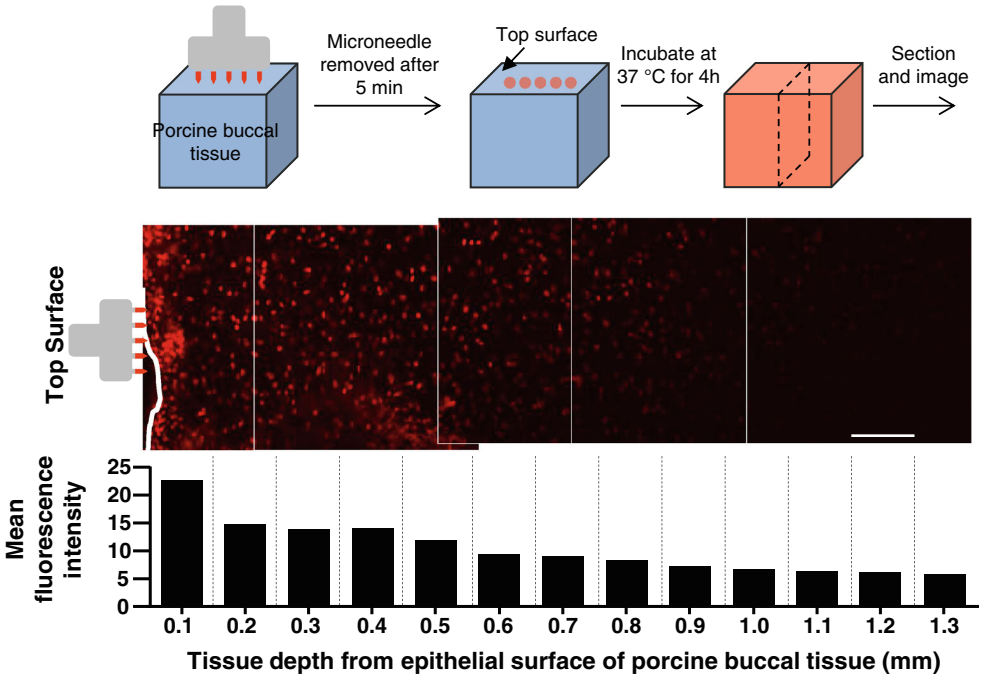

Fig. 6 Delivery of DOX in porcine buccal tissue after insertion of 1D microneedle arrays coated with DOX-PLGA nanoparticles. Montage of individual confocal fluorescent micrographs from a representative transverse section of porcine buccal mucosa characterizing distribution of DOX along the depth. *Bar graph* shows variation in the mean fluorescence intensity as a function of depth from the insertion site. Scale bar represents: 100 μm

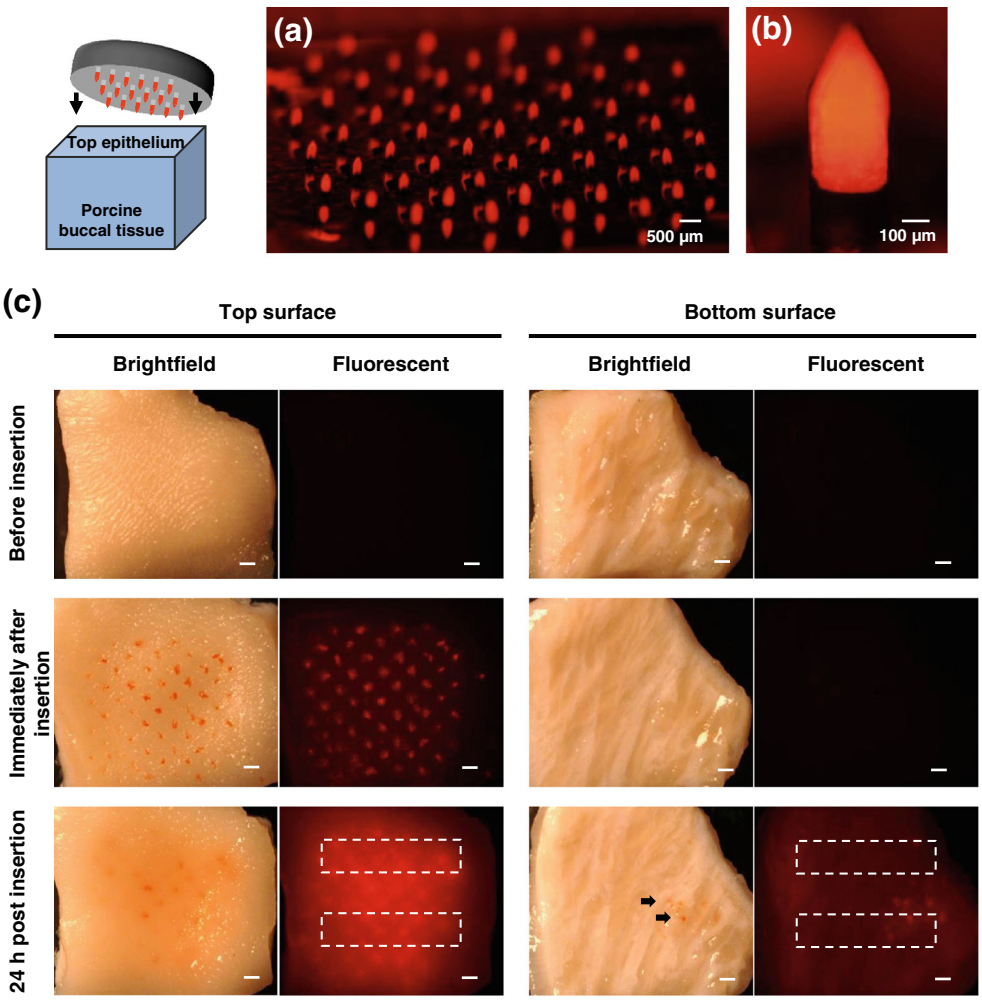

Fig. 7 Delivery of DOX in porcine buccal tissue after insertion of a 2D microneedle array coated with free DOX. (**a**) Fluorescent stereomicrograph of a 2D microneedle array coated with free DOX. (**b**) Zoom up of a representative microneedle of the 2D microneedle array coated with free DOX. (**c**) Brightfield and fluorescent stereomicrographs of top and bottom surfaces of a representative whole porcine buccal tissue before microneedle array insertion, immediately after insertion and 24 h post insertion. *Arrows* point to DOX that has diffused to the backside of the tissue after 24 h. *Dotted rectangles* indicate representative areas of the tissue whose mean fluorescence intensity was compared to the mean fluorescence intensity across the entire area of the respective tissue, to evaluate uniformity of DOX distribution. Less than 10 % variation in mean fluorescence intensity between the dotted area and the entire respective tissue area was observed. All *scale bars* in (**C**) represent: 1 mm

fluorescence. At 24 h post insertion, the tissue presented less obvious presence of DOX across the top surface under brightfield conditions, but a uniform distribution of DOX was seen under fluorescent conditions. Fluorescence uniformity was confirmed by measuring mean fluorescence intensity of the treated area and selected regions within it. The variation in the mean fluorescence intensity of the selected regions of interests was found to be less than 10 % of the average mean fluorescence intensity of the tissue. Simultaneously, under brightfield conditions, the bottom tissue-surface illustrates a minimal presence of DOX resulting from diffusion as seen by the red specks (pointed by arrows), whereas the fluorescent image shows uniform distribution of DOX across the entire back surface. Similar to the top surface, the variation in the mean fluorescence intensity of the selected regions was less than 10 % of the mean fluorescence intensity of the entire bottom tissue surface. During this 24 h period while DOX diffused, no significant amount leaked from the bottom of the tissue.

This experiment demonstrates the ability of microneedle-deposited DOX to diffuse uniformly in the volume of a porcine buccal tissue measuring 1 cm x 1 cm x 4 mm, *in vitro*. Oral tumor thickness can vary widely depending on tumor stage, ranging from 2 to 5 mm to as high as 9–10 mm (Huang et al. 2009; Kademani 2007; Pentenero et al. 2005). The result of this experiment is thus exciting because it suggests that coated microneedles have the potential for intratumoral drug delivery, and while the microneedle are less than a mm long, they can certainly potentiate drug delivery deeper into the oral tissue by diffusion.

3.7 Leakage of injected fluid from porcine cadaver buccal tissues

Hypodermic injections are currently used for intratumoral drug delivery. Injections are however known to cause leakage of fluid from injected site into neighboring blood vessels, which can lead to systemic delivery and potentially harmful

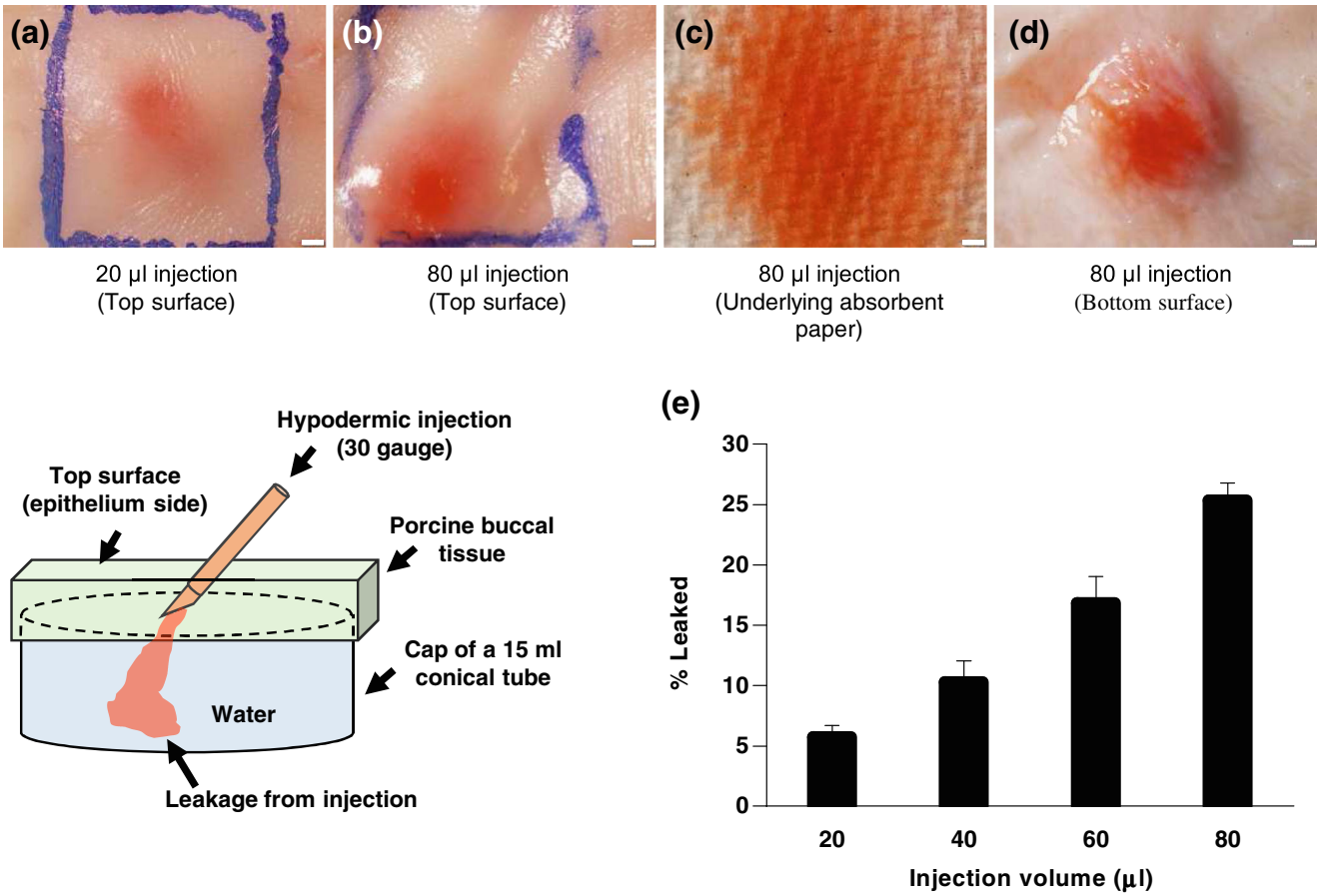

Fig. 8 Leakage of fluid from porcine buccal tissue after hypodermic injection. (**a**) Brightfield stereomicrograph of top surface of porcine buccal tissue after 20 µl injection of DOX solution. (b) Brightfield stereomicrograph of top surface of porcine buccal tissue after 80 µl injection of DOX solution. Marked regions in (**a**) and (**b**) represent an area approximately the size of the 2D microneedle array to help put into perspective the size of the injected area. (**c**) Brightfield stereomicrograph of paper pad placed under the porcine buccal tissue during injection of 80 µl DOX solution to qualitatively show fluid has leaked from the bottom during injection. (**d**) Brightfield stereomicrograph of bottom surface of porcine buccal tissue after 80 µl injection of DOX solution. (**e**) Percentage of injected DOX solution that leaks from the bottom of the porcine buccal tissue as a function of injected volume. All *scale bars* represent: 1 mm

side effects (Castro et al. 2003). We quantified the fraction of injected liquid that leaks out from tissues by injecting 20, 40, 60 and 80 μl into a porcine cadaver tissue. From Fig. 8a it can be seen that a 20 μl injection into the same area as the 2 D microneedles array does not lead to uniform delivery. At a higher injection volume of 80 μl, a larger bleb was formed on the tissue surface, however, the fluid did not still distribute well in the tissue (Fig. 8b). Some volume leaked from the bottom of the tissue as can be seen from the stain formed on a paper pad placed underneath the tissue during injection (Fig. 8c). The underside of the tissue from where the fluid leaked is shown in Fig. 8d. Quantification of the leakage volume shows that the percentage of injected volume that leaks increases with injection volume. About 25 % of the injected fluid leaked out for an 80 μl injection volume (Fig. 8e).

This experiment establishes the difficulty associated with hypodermic injections in to tissues without causing leakage of fluid. Due to limited capacity of tissues to imbibe injected fluids, leakage effects were observed. We could not inject a 100 μl volume in to the tissue reliably because the fluid leaked both from the top and the bottom surfaces of the tissue. However, in phase III clinical trials volumes up to 50 ml in increments of 2.5 ml have been injected into tumors of patients (Castro et al. 2003). Based on our experimental result it is expected that retention of such large volumes of fluids within the tumors would be short lived. Indeed, in a mouse study with human pancreatic cancer xenografts, it was found that immediately after injection of a 50 μl volume of 5-fluorouracil into the tumor, only 39 % of the injected volume was retained (Smith et al. 1999). After 0.5 h and 1 h the dose remaining in the tissue was just 0.9 and 0.22 %, respectively. Even injection of a collagen gel containing 5-fluorouracil did not enhance retention significantly—only 15 % 5-fluorouracil remained after 2 h and 1 % after 4 h of intratumoral injection. In contrast coated microneedle arrays do not involve fluid injection, and can thus significantly reduce drug loss from tumors. Further, the closely-spaced microneedles allow uniform delivery of drugs in to tissues, as seen in Fig. 8c. Thus, coated microneedles can be a more promising method for local targeting of drugs to oral tumors.

4 Conclusion

In summary, this study demonstrates that microneedles coated with drug-encapsulating nanoparticles can be an attractive method for localized drug delivery to tumors of the oral cavity. To demonstrate this concept, DOX-PLGA nanoparticles with an average diameter of 137 nm, and EE and LE of 4.41 and 1.8 %, respectively, were synthesized. DOX-PLGA nanoparticles were uniformly coated on microneedles. The dose of DOX-PLGA on a 1D microneedle array containing 5 microneedles was found to be approximately 0.6 μg, which based on calculations was expected to provide sufficient dose of DOX to be toxic to cancer cells situated within a 1 cm^3 tissue. Microscopic evaluation of 3D tissue phantoms treated with 1D microneedle arrays that were coated with DOX-PLGA nanoparticles demonstrated that DOX upon release from nanoparticles could diffuse about 1–2 mm laterally from the insertion point, and up to 3 mm deep into the tissue. Cytotoxicity evaluation further showed that DOX can result in cell death in 3D tissue phantoms. Using confocal and stereo microscopy, the ability of DOX to diffuse in porcine cadaver tissues up to a depth of about 4 mm and laterally in an area measuring 1 cm x 1 cm was also demonstrated. Lastly, leakage of fluid during tissue injections was quantified to demonstrate that intratumoral injections suffer from drug leakage issues, which can result in rapid depletion of drug from the injected area and systemic side effects. In contrast to injections, coated microneedles do not involve fluid injections, and can deliver drug at controlled and well distributed locations in the tissue, resulting in an overall better performance compared to hypodermic needles. Thus, this study supports the concept that coated microneedle arrays can offer a convenient microscale drug delivery device, which has potential to be used by clinicians for local delivery of cancer therapeutics to tumor tissues.

Acknowledgments This work was supported in part by the High-Impact/High-Risk Research Award to HSG from the Cancer Prevention and Research Institute of Texas (CPRIT). HSG is a co-inventor on a patent related to microneedle coating technology. The patent application is still pending in the US patent office.

Conflict of interest This potential conflict of interest has been disclosed and is managed by Texas Tech University.

References

E.B. Brown, Y. Boucher, S. Nasser, R.K. Jain, Measurement of macromolecular diffusion coefficients in human tumors. Microvasc. Res. **67**, 231–236 (2004)

H.A. Burris III, C.L. Vogel, D. Castro, L. Mishra, M. Schwarz, S. Spencer, D.D. Oakes, R. KOREY, E.K. Orenberg, Intratumoral cisplatin/epinephrine-injectable gel as a palliative treatment for accessible solid tumors: a multicenter pilot study. Otolaryngol. Head Neck Surg. **118**, 496–503 (1998)

D.J. Castro, K.S. Sridhar, H.S. Garewal, G.M. Mills, B.L. Wenig, F.R. Dunphy 2nd, P.D. Costantino, R.D. Leavitt, M.E. Stewart, E.K. Orenberg, Intratumoral cisplatin/epinephrine gel in advanced head and neck cancer: a multicenter, randomized, double-blind, phase III study in North America. Head Neck **25**, 717–731 (2003)

V.P. Chauhan, R.M. Lanning, B. Diop-Frimpong, W. Mok, E.B. Brown, T.P. Padera, Y. Boucher, R.K. Jain, Multiscale measurements distinguish cellular and interstitial hindrances to diffusion *in vivo*. Biophys. J. **97**, 330–336 (2009)

C.T. Chen, J.L.S. Au, M.G. Wientjes, Pharmacodynamics of doxorubicin in human prostate tumors. Clin. Cancer Res. **4**, 277–282 (1998)

L.Y. Chu, S.O. Choi, M.R. Prausnitz, Fabrication of dissolving polymer microneedles for controlled drug encapsulation and delivery:

Bubble and pedestal microneedle designs. J. Pharm. Sci. **99**, 4228–4238 (2010)

G.L. Clayman, A.K. El-Naggar, S.M. Lippman, Y.C. Henderson, M. Frederick, J.A. Merritt, L.A. Zumstein, T.M. Timmons, T.-J. Liu, L. Ginsberg, Adenovirus-mediated p53 gene transfer in patients with advanced recurrent head and neck squamous cell carcinoma. J. Clin. Oncol. **16**, 2221–2232 (1998)

B.D. Curti, W.J. Urba, W. Gregory Alvord, J.E. Janik, J.W. Smith, K. Madara, D.L. Longo, Interstitial pressure of subcutaneous nodules in melanoma and lymphoma patients: changes during treatment. Cancer Res. **53**, 2204–2207 (1993)

P.C. DeMuth, P.T. Hammond, D.J. Irvine, Transcutaneous delivery of plasmid DNA and degradable polymer nanoparticles from multilayer-coated microneedle arrays. Abstr. Pap. Am. Chem. S. **240** (2010)

M.E. Devries, H.E. Bodde, J.C. Verhoef, M. Ponec, W.I.H.M. Craane, H.E. Junginger, Localization of the permeability barrier inside porcine buccal mucosa—a combined invitro study of drug permeability, electrical-resistance and tissue morphology. Int. J. Pharm. **76**, 25–35 (1991)

F.A. Fornari, J.K. Randolph, J.C. Yalowich, M.K. Ritke, D.A. Gewirtz, Interference by doxorubicin with DNA unwinding in MCF-7 breast tumor cells. Mol. Pharmacol. **45**, 649–656 (1994)

J.T. French, B. Goins, M. Saenz, S. Li, X. Garcia-Rojas, W.T. Phillips, R.A. Otto, A. Bao, Interventional therapy of head and neck cancer with lipid nanoparticle-carried rhenium 186 radionuclide. J. Vasc. Interv. Radiol. **21**, 1271–1279 (2010)

H.S. Gill, M.R. Prausnitz, Coated microneedles for transdermal delivery. J. Control. Release **117**, 227–237 (2007)

H.S. Gill, D.D. Denson, B.A. Burris, M.R. Prausnitz, Effect of microneedle design on pain in human volunteers. Clin. J. Pain **24**, 585–594 (2008)

H.S. Gill, J. Soderholm, M.R. Prausnitz, M. Sallberg, Cutaneous vaccination using microneedles coated with hepatitis C DNA vaccine. Gene Ther. **17**, 811–814 (2010)

S.D. Gittard, A. Ovsianikov, N.A. Monteiro-Riviere, J. Lusk, P. Morel, P. Minghetti, C. Lenardi, B.N. Chichkov, R.J. Narayan, Fabrication of polymer microneedles using a two-photon polymerization and micromolding process. J. Diabetes Sci. Technol. **3**, 304–311 (2009)

D.K. Goette, R.B. Odom, Successful treatment of keratoacanthoma with intralesional fluorouracil. J. Am. Acad. Dermatol. **2**, 212–216 (1980)

R. Gutmann, M. Leunig, J. Feyh, A.E. Goetz, K. Messmer, E. Kastenbauer, R.K. Jain, Interstitial hypertension in head and neck tumors in patients: correlation with tumor size. Cancer Res. **52**, 1993–1995 (1992)

R.I. Haddad, D.M. Shin, Recent advances in head and neck cancer. N. Engl. J. Med. **359**, 1143–1154 (2008)

S.B. Hancock, G.A. Krempl, V. Canfield, C. Bogardus, K. Kojouri, S.K. Kaneaster, J.E. Medina, Treatment of base of tongue cancer with paclitaxel, ifosfamide, and cisplatinum induction chemotherapy followed by chemoradiotherapy. Laryngoscope **118**, 1357–1361 (2008)

C.-H. Heldin, K. Rubin, K. Pietras, A. Ostman, High interstitial fluid pressure—an obstacle in cancer therapy. Nat. Rev. Cancer **4**, 806–813 (2004)

R. Hitt, Induction chemotherapy in head and neck cancer. Ann. Oncol. **17**(Suppl 10), 42–44 (2006)

R. Hitt, J.J. Grau, A. Lopez-Pousa, A. Berrocal, C. Garcia-Giron, A. Irigoyen, J. Sastre, J. Martinez-Trufero, J.A. Brandariz Castelo, E. Verger, J.J. Cruz-Hernandez, A randomized phase III trial comparing induction chemotherapy followed by chemoradiotherapy versus chemoradiotherapy alone as treatment of unresectable head and neck cancer. Ann. Oncol. **25**, 216–225 (2014)

S.H. Huang, D. Hwang, G. Lockwood, D.P. Goldstein, B. O'Sullivan, Predictive value of tumor thickness for cervical lymph-node involvement in squamous cell carcinoma of the oral cavity a meta-analysis of reported studies. Cancer **115**, 1489–1497 (2009)

R.A. Jain, The manufacturing techniques of various drug loaded biodegradable poly(lactide-co-glycolide) (PLGA) devices. Biomaterials **21**, 2475–2490 (2000)

D. Kademani, Oral cancer. Mayo Clin. Proc. **82**, 878–887 (2007)

F.R. Khuri, J. Nemunaitis, I. Ganly, J. Arseneau, I.F. Tannock, L. Romel, M. Gore, J. Ironside, R. MacDougall, C. Heise, A controlled trial of intratumoral ONYX-015, a selectively-replicating adenovirus, in combination with cisplatin and 5-fluorouracil in patients with recurrent head and neck cancer. Nat. Med. **6**, 879–885 (2000a)

F.R. Khuri, D.M. Shin, B.S. Glisson, S.M. Lippman, W.K. Hong, Treatment of patients with recurrent or metastatic squamous cell carcinoma of the head and neck: current status and future directions. Semin. Oncol. **27**, 25–33 (2000b)

Y.C. Kim, F.S. Quan, R.W. Compans, S.M. Kang, M.R. Prausnitz, Formulation and coating of microneedles with inactivated influenza virus to improve vaccine stability and immunogenicity. J. Control. Release **142**, 187–195 (2010)

U. Kulkarni, R. Mahalingam, I. Pather, X.L. Li, B. Jasti, Porcine buccal mucosa as *in vitro* model: effect of biological and experimental variables. J. Pharm. Sci. **99**, 1265–1277 (2010)

H.A. Leddy, M.A. Haider, F. Guilak, Diffusional anisotropy in collagenous tissues: fluorescence imaging of continuous point photobleaching. Biophys. J. **91**, 311–316 (2006)

J.W. Lee, Han, M.R., Park, J.H. Polymer microneedles for transdermal drug delivery. J. Drug Target (2012)

Z. Luo, T. Ye, Y. Ma, H.S. Gill, N. Nitin, Microprecision delivery of oligonucleotides in a 3D tissue model and its characterization using optical imaging. Mol. Pharm. **10**, 2868–2879 (2013)

Y. Ma, Tao, W., Krebs, S.J., Sutton, W.F., Haigwood, N.L., Gill, H.S. Vaccine delivery to the oral cavity using coated microneedles induces systemic and mucosal immunity. Pharm. Res. (2014)

G.C. MacDonald, M. Rasamoelisolo, J. Entwistle, J. Cizeau, D. Bosc, A phase I clinical study of VB4-845: Weekly intratumoral administration of an anti-EpCAM recombinant fusion protein in patients with squamous cell carcinoma of the head and neck. Drug. Des. Devel. Ther. **2**, 105–114 (2008)

G.C. MacDonald, M. Rasamoelisolo, J. Entwistle, W. Cuthbert, M. Kowalski, M.A. Spearman, N. Glover, A phase I clinical study of intratumorally administered VB4-845, an anti-epithelial cell adhesion molecule recombinant fusion protein, in patients with squamous cell carcinoma of the head and neck. Med. Oncol. **26**, 257–264 (2009)

M. Milosevic, A. Fyles, D. Hedley, R. Hill, The human tumor microenvironment: invasive (needle) measurement of oxygen and interstitial fluid pressure. Semin. Radiat. Oncol. **14**, 249–258 (2004)

A. Miyazaki, J. Kobayashi, T. Torigoe, Y. Hirohashi, T. Yamamoto, A. Yamaguchi, H. Asanuma, A. Takahashi, Y. Michifuri, K. Nakamori, Phase I clinical trial of survivin-derived peptide vaccine therapy for patients with advanced or recurrent oral cancer. Cancer Sci. **102**, 324–329 (2011)

H. Mizutani, S. Tada-Oikawa, Y. Hiraku, M. Kojima, S. Kawanishi, Mechanism of apoptosis induced by doxorubicin through the generation of hydrogen peroxide. Life Sci. **76**, 1439–1453 (2005)

I. Müller, A. Jenner, G. Bruchelt, D. Niethammer, B. Halliwell, Effect of concentration on the cytotoxic mechanism of doxorubicin—apoptosis and oxidative DNA damage. Biochem. Biophys. Res. Commun. **230**, 254–257 (1997)

J. Nemunaitis, F. Khuri, I. Ganly, J. Arseneau, M. Posner, E. Vokes, J. Kuhn, T. McCarty, S. Landers, A. Blackburn, Phase II trial of intratumoral administration of ONYX-015, a replication-selective adenovirus, in patients with refractory head and neck cancer. J. Clin. Oncol. **19**, 289–298 (2001)

J.J. Norman, M.R. Brown, N.A. Raviele, M.R. Prausnitz, E.I. Felner, Faster pharmacokinetics and increased patient acceptance of

intradermal insulin delivery using a single hollow microneedle in children and adolescents with type 1 diabetes. Pediatr. Diabetes **14**, 459–465 (2013)

J.H. Park, M.G. Allen, M.R. Prausnitz, Biodegradable polymer microneedles: fabrication, mechanics and transdermal drug delivery. J. Control. Release **104**, 51–66 (2005)

M. Pentenero, S. Gandolfo, M. Carrozzo, Importance of tumor thickness and depth of invasion in nodal involvement and prognosis of oral squamous cell carcinoma: a review of the literature. Head Neck **27**, 1080–1091 (2005)

B. Raju, Ibrahim, S.O., Pathophysiology of oral cancer in experimental animal models: a review with focus on the role of sympathetic nerves. J. Oral. Pathol. Med. **40**(1), 1-9 (2011)

S. Ramanujan, A. Pluen, T.D. McKee, E.B. Brown, Y. Boucher, R.K. Jain, Diffusion and convection in collagen gels: implications for transport in the tumor interstitium. Biophys. J. **83**, 1650–1660 (2002)

E.K. Rofstad, E.-B.M. Ruud, B. Mathiesen, K. Galappathi, Associations between radiocurability and interstitial fluid pressure in human tumor xenografts without hypoxic tissue. Clin. Cancer Res. **16**, 936–945 (2010)

K. Shahani, S.K. Swaminathan, D. Freeman, A. Blum, L. Ma, J. Panyam, Injectable sustained release microparticles of curcumin: a new concept for cancer chemoprevention. Cancer Res. **70**, 4443–4452 (2010)

J.P. Smith, S. Kanekal, M.B. Patawaran, J.Y. Chen, R.E. Jones, E.K. Orenberg, N.Y. Yu, Drug retention and distribution after intratumoral chemotherapy with fluorouracil/epinephrine injectable gel in human pancreatic cancer xenografts. Cancer Chemother. Pharmacol. **44**, 267–274 (1999)

K. Sokolov, J. Galvan, A. Myakov, A. Lacy, R. Lotan, R. Richards-Kortum, Realistic three-dimensional epithelial tissue phantoms for biomedical optics. J. Biomed. Opt. **7**, 148–156 (2002)

S.P. Sullivan, D.G. Koutsonanos, M.D. Martin, J.W. Lee, V. Zarnitsyn, S.O. Choi, N. Murthy, R.W. Compans, I. Skountzou, M.R. Prausnitz, Dissolving polymer microneedle patches for influenza vaccination. Nat. Med. **16**, 915–U116 (2010)

F. Tewes, E. Munnier, B. Antoon, L. Ngaboni Okassa, S. Cohen-Jonathan, H. Marchais, L. Douziech-Eyrolles, M. Soucé, P. Dubois, I. Chourpa, Comparative study of doxorubicin-loaded poly (lactide-co-glycolide) nanoparticles prepared by single and double emulsion methods. Eur. J. Pharm. Biopharm. **66**, 488–492 (2007)

K. van der Maaden, S.J. Trietsch, H. Kraan, E.M. Varypataki, S. Romeijn, R. Zwier, H.J. van der Linden, G. Kersten, T. Hankemeier, W. Jiskoot, J. Bouwstra, Novel hollow microneedle technology for depth-controlled microinjection-mediated dermal vaccination: a study with polio vaccine in rats. Pharm. Res. **31**, 1846–1854 (2014)

P.C. Wang, S.J. Paik, S.D. Chen, S. Rajaraman, S.H. Kim, M.G. Allen, Fabrication and characterization of polymer hollow microneedle array using UV lithography into micromolds. J. Microelectromech. S. **22**, 1041–1053 (2013)

P.W. Wertz, C.A. Squier, Cellular and molecular-basis of barrier function in oral epithelium. Crit. Rev. Ther. Drug. **8**, 237–269 (1991)

G. Widera, J. Johnson, L. Kim, L. Libiran, K. Nyam, P.E. Daddona, M. Cormier, Effect of delivery parameters on immunization to ovalbumin following intracutaneous administration by a coated microneedle array patch system. Vaccine **24**, 1653–1664 (2006)